From bi-dimensional discrete model to anisotropic damage model: a feasibility study

Flavien Loiseau, Rodrigue Desmorat, Cécile Oliver-Leblond

▶ **To cite this version:**

Flavien Loiseau, Rodrigue Desmorat, Cécile Oliver-Leblond. From bi-dimensional discrete model to anisotropic damage model: a feasibility study. Congrès Français de Mécanique, Aug 2022, Nantes, France. hal-03892314

HAL Id: hal-03892314
https://hal.science/hal-03892314

Submitted on 9 Dec 2022

HAL is a multi-disciplinary open access archive for the deposit and dissemination of scientific research documents, whether they are published or not. The documents may come from teaching and research institutions in France or abroad, or from public or private research centers.

L'archive ouverte pluridisciplinaire **HAL**, est destinée au dépôt et à la diffusion de documents scientifiques de niveau recherche, publiés ou non, émanant des établissements d'enseignement et de recherche français ou étrangers, des laboratoires publics ou privés.

From bi-dimensional discrete model to anisotropic damage model : a feasibility study

F. Loiseau, R. Desmorat, C. Oliver-Leblond

Université Paris-Saclay, CentraleSupélec, ENS Paris-Saclay, CNRS, Laboratoire de Mécanique Paris-Saclay, 91190, Gif-sur-Yvette, France.
(Email: flavien.loiseau@ens-paris-saclay.fr, rodrigue.desmorat@ens-paris-saclay.fr, cecile.oliver@ens-paris-saclay.fr)

Résumé :

Ce travail étudie l'utilisation d'un modèle discret (qui représente explicitement la fissuration) comme une "machine d'essai virtuelle". En général, des expériences complexes sont requises pour formuler et identifier les modèles d'endommagement anisotropes. L'utilisation d'un modèle discret permettrait de réduire de coût experimental nécessaire à la formulation d'un modèle discret. Dans cette étude, un modèle beam-particle *représente une éprouvette bidimensionnelle carrée. Un chargement endommageant est appliqué sur l'éprouvette jusqu'à la localisation de la micro-fissuration. L'évolution du tenseur d'élasticité effectif est mesurée à chaque instant via des chargements de mesure élastiques. Pour conclure, la procédure est illustrée sur un cas de traction. La décomposition harmonique est utilisée pour analyser les résultats. Cette analyse montre la correlation entre micro-fissuration et perte de rigidité. De plus, les calculs des distances aux classes de symétries permettent de quantifier l'anisotropie induite par la micro-fissuration. Cette étude pose les bases d'un projet plus complet visant à construire un modèle d'endommagement anisotrope basé sur la décomposition harmonique.*

Abstract :

This study investigates using a discrete model (explicitly representing micro-cracking) as a "virtual test machine". Anisotropic damage models often require complex experiments to be formulated and identified. Discrete models could reduce the experimental cost of formulating an anisotropic damage model. A beam particle model represents a 2D square specimen of quasi-brittle material in this work. A damaging loading is applied to the specimen until the localization of micro-cracking. The evolution of the effective elasticity tensor is measured at each load step through elastic loadings. The measurement procedure is then illustrated with a tensile loading. Harmonic decomposition is used to analyze this evolution. The analysis of the evolution highlights the correlation between micro-cracking and stiffness loss. Additionally, calculating distances to symmetry classes allows quantifying anisotropy induced by micro-cracking. Eventually, it will provide a means to build an anisotropic damage model based on harmonic decomposition.

Keywords : damage, anisotropy, elasticity tensor, discrete beam-particle model, harmonic decomposition.

1 Introduction

Quasi-brittle materials are massively used in civil engineering applications. Predicting their mechanical degradation is necessary to guarantee the integrity of a structure. The primary mechanism of mechanical degradation for such materials is the nucleation of micro-cracks that grow and merge into macro-cracks. Even if the material is initially isotropic, it may become anisotropic due to micro-cracks orientation. Thus, anisotropic damage models are interesting to describe this behavior [1, 2]. Nevertheless, these models generally require complex experimental procedures to be formulated and identified. An alternative method consists in using models describing the material behavior at the microscale. Such models have been used to (partially or entirely) formulate and identify a macroscopic behavior law ([3, 4, 5] among others). A good candidate to represent quasi-brittle materials at a micro-scale is the beam-particle model [6, 3, 7]. It combines a lattice model with a particulate model. The lattice part of the model represents the elastic behavior [8] and the failure of the material [9, 10]). The particular part of the model [11] represents the contact and sliding between crack faces. For instance, [3] uses a beam-particle model to identify an anisotropic damage model's parameter (requiring complex loading). This work aims at completing and extending the work of [12]. This work is the first step to formulating an anisotropic damage model from micromechanical simulations. In particular, it aims at exploring the use of a discrete model to formulate an anisotropic damage model.

The first section introduces the harmonic decomposition of the elasticity tensor and distance to symmetry classes. Those tools are used to describe and analyze elasticity tensors. The second section presents the beam-particle model. The third section introduces the method to measure effective elasticity tensors from the discrete simulations. Finally, the evolution of elasticity tensor over damaging loadings is obtained and analyzed.

2 Analysis of elasticity tensors

2.1 Harmonic decomposition

The harmonic decomposition of the elasticity tensor is a mathematical tool introduced by [13]. In 2D, it states that any elasticity tensor $\mathbf{E} \in \mathbb{E}\mathrm{la}(\mathbb{R}^2)$ is decomposable into a quadruplet:

$$\mathbf{E} = (\mu, \kappa, \mathbf{d}', \mathbf{H}) \in \mathbb{E}\mathrm{la}(\mathbb{R}^2) \tag{1}$$

where μ is the shear modulus, κ is the bulk modulus (in 2D), $\mathbf{d}$ is a second-order tensor named dilatation tensor, and $\mathbf{H}$ is a fourth-order tensor named harmonic part. It is essential to notice that $\mathbf{d}'$ and $\mathbf{H}$ are harmonic tensors (traceless and totally symmetric). They are both entirely defined by two independent variables: $\mathbf{d}'_{11}$ and $\mathbf{d}'_{12}$ for $\mathbf{d}'$, $\mathbf{H}_{1111}$ and $\mathbf{H}_{1112}$ for $\mathbf{H}$.

The shear modulus μ and the bulk modulus κ are invariant by rotation of the elasticity tensor. $\mathbf{d}'$ and $\mathbf{H}$ are covariant by rotation of the elasticity tensor. Consider $g(\theta) \in \mathbf{SO}(\mathbb{R}^2)$ a rotation in $\mathbb{R}^2$, the invariance and covariance properties mean that:

$$g(\theta) \star \mathbf{E}(\mu, \kappa, \mathbf{d}', \mathbf{H}) = \mathbf{E}(\mu, \kappa, g(\theta) \star \mathbf{d}', g(\theta) \star \mathbf{H}) \tag{2}$$

Given a decomposition $(\mu, \kappa, \mathbf{d}', \mathbf{H})$, the reconstruction formula is:

$$\mathbf{E} = \mathbf{E}_{\text{iso}}(\mu,\kappa) + \mathbf{E}_{\text{dil}}(\mathbf{d}') + \mathbf{H} \qquad \text{where:} \quad \begin{cases} \mathbf{E}_{\text{iso}}(\mu,\kappa) = 2\mu\mathbf{J} + \kappa\mathbf{1}\otimes\mathbf{1} & \text{isotropic part} \\ \mathbf{E}_{\text{dil}}(\mathbf{d}') = \frac{1}{2}\left(\mathbf{d}'\otimes\mathbf{1} + \mathbf{1}\otimes\mathbf{d}'\right) & \text{dilatation part} \\ \mathbf{H} = \mathbf{E} - \mathbf{E}_{\text{iso}}(\mu,\kappa) - \mathbf{E}_{\text{dil}}(\mathbf{d}') & \text{harmonic part} \end{cases} \tag{3}$$

where $\mathbf{1}$ is the second order identity, $\mathbf{J}$ is the deviatoric projector ($\mathbf{J} = \mathbf{I} - \frac{1}{2}\mathbf{1}\otimes\mathbf{1}$), and $\mathbf{I}$ is the fourth order symmetric identity ($I_{ijkl} = \frac{1}{2}\left(\delta_{ik}\,\delta_{jl} + \delta_{il}\delta_{jk}\right)$).

Given an elasticity tensor $\mathbf{E} \in \mathbb{E}\text{la}(\mathbb{R}^2)$, the expressions of the coefficients of the decomposition are:

$$\mu = \frac{1}{8}\left(2\text{tr}(\mathbf{v}) - \text{tr}(\mathbf{d})\right) \tag{4}$$

$$\kappa = \frac{1}{4}\text{tr}(\mathbf{d}) \tag{5}$$

$$\mathbf{d}' = \mathbf{d} - \frac{1}{2}\text{tr}(\mathbf{d})\mathbf{1} \tag{6}$$

$$\mathbf{H} = \mathbf{E} - \mathbf{E}_{\text{iso}}(\mu,\kappa) - \mathbf{E}_{\text{dil}}(\mathbf{d}') \tag{7}$$

where $\mathbf{d} = \text{tr}_{12}(\mathbf{E})$ is the dilation tensor (indicial notation: $\left(\text{tr}_{12}(\mathbf{E})\right)_{ij} = E_{kkij}$), and $\mathbf{v} = \text{tr}_{13}(\mathbf{E})$ is the Voigt tensor (indicial notation: $\left(\text{tr}_{13}(\mathbf{E})\right)_{ij} = E_{kikj}$).

2.2 Distance to a symmetry class

Given an elasticity tensor $\mathbf{E}$, the objective is to determine the closest elasticity tensor $\mathbf{E}_{\mathcal{C}}$, having a specific symmetry classe $\mathcal{C}$. This problem can be expressed as a minimization problem:

$$\mathbf{E_C} = \underset{\mathbf{E}^* \in \mathcal{C}}{\arg\min} \frac{\|\mathbf{E} - \mathbf{E}^*\|}{\|\mathbf{E}\|} \tag{8}$$

A parametrization of the constrained elasticity tensor $\mathbf{E}*$ is interesting to solve this problem. A method consists in using the normal form $\mathbf{N}^{\mathcal{C}}$ associated to symmetry class $\mathcal{C}$ rotated by an angle θ. For instance, for the orthotropic class:

$$\mathbf{N}^{\mathcal{C}} = \begin{bmatrix} N_{1111} & N_{1122} & \sqrt{2}N_{1112} \\ N_{1122} & N_{2222} & \sqrt{2}N_{1222} \\ \sqrt{2}N_{1112} & \sqrt{2}N_{1222} & 2N_{1222} \end{bmatrix} \implies \mathbf{E}^* = \mathbf{R}^T(\theta)\mathbf{N}^{\mathcal{C}}\mathbf{R}(\theta) \tag{9}$$

For the isotropic class, this problem can be solved analytically using the harmonic decomposition. Indeed, the closest isotropic elasticity tensor of $\mathbf{E}$ is its isotropic part $\mathbf{E}_{\text{iso}}$. For the orthotropic class, calculations details are provided by [14]. This case is more more complicated since the minimization problem leads to finding the roots of a 8th order real polynomial. The root-finding problem can be solved using symbolic calculations.

3 Beam-particle model

As complex measurements and experiments are required for this study, a beam-particle model is used to represent a quasi-brittle material. This section is dedicated to the presentation of this model.

3.1 Presentation

The Figure 1 is an illustratation of the model's mesh. The mesh consists in a set of randomly placed rigid particles. The particles are linked by Euler-Bernoulli beams to model the cohesion.

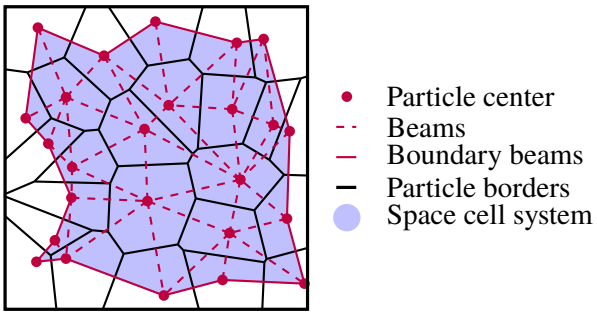

Figure 1: Representation of beam-particle mesh

Each beam (pq), linking particles p and q, has an Euler-Bernoulli behavior and is parametrized by its length l_{pq}, section A_{pq}, Young modulus E, and coefficient of inertia $\alpha_{pq} = {}^{64I_b\pi}/_{A_b^2}$. l_{pq} and A_{pq} are obtained from the mesh's geometry and thus change for each beam. E and α_{pq} are constant for all beams and identified to match a macroscopic behavior.

Adding a brittle failure criterion to each beams provides macroscopic fracture properties. The failure of a beam is governed by a combination its tension and bending. It allows to model the macroscopic dissymmetry in tension-compression [7]. In order to obtain a quasi-brittle macroscopic behavior, tension and bending thresholds are randomly drawn for each beam.

The parameters of the discrete model are identified to reproduce the behavior of a mortar with the following parameters: Young's modulus $E = 36.35$ GPa, Poisson ratio $\nu = 0.22$, tensile strength $f_t = 3$ MPa and compressive strength $f_c = 40$ MPa. The elastic properties are equivalent to a bulk modulus $\kappa = 23.24$ GPa and a shear modulus $\mu = 14.92$ GPa.

3.2 Periodic boundary conditions

The measure of the elasticity tensor of a Representative Area Element (RAE) uses Periodic Boundary Conditions (PBC). For this study, PBC are enforced by adding guided particles constrained to follow the movement of guiding particles. The mesh must be modified to introduce guided particles having the same geometry as the associated guiding particles. The guided particle's movement $\mathbf{u}_p$ relates to the guiding particle movement's $\mathbf{u}_q$ through: $\mathbf{u}_p = \bar{\boldsymbol{\varepsilon}}_d(\mathbf{x}_p - \mathbf{x}_q) + \mathbf{u}_q$, where $\bar{\boldsymbol{\varepsilon}}_d$ is the imposed strain. In the linear system associated to the model, this relation is enforced through Lagrange multipliers.

4 Measurement of the evolution of effective elasticity tensors

4.1 Measurement of an effective elasticity tensor

The definition of the elasticity tensor is based on continuous quantities (stress and strain), which are undefined in a discrete framework. Bagi [15] analyzes several definitions of average strain for 2D discrete models. This work uses the average strain $\bar{\boldsymbol{\varepsilon}}$ proposed by [16] and recalled in Equation 10.

$$\bar{\boldsymbol{\varepsilon}} = \frac{1}{S} \sum_{b \in \mathcal{B}_b} \left(\frac{\mathbf{u}_{b(1)} + \mathbf{u}_{b(2)}}{2} \odot \mathbf{n}_b \right) l_b \tag{10}$$

where $\odot$ is the symmetrized tensor product, S is the area [1] of the RAE, $\mathcal{B}_b$ is the set of boundary beams, $b(i)$ is the ith particle of beam b, $\mathbf{u}_p$ is the displacement of particle p, $\mathbf{n}_b$ is the outward-pointing normal of beam b, and $\mathbf{l}_b$ is the length of beam b. The average Cauchy stress tensor $\bar{\boldsymbol{\sigma}}$ is calculated using a

[1] This area corresponds to the "effective mechanical area", or space cell system (see Figure 1).

symmetrized[2] version of the definition proposed by [16]:

$$\bar{\boldsymbol{\sigma}} = \frac{1}{S} \sum_{p \in \mathcal{P}_b} \mathbf{f}_p \odot \mathbf{x}_p \tag{11}$$

where $\mathcal{P}_b$ is the set of boundary particles, $\mathbf{f}_p$ is the resulting force on particle p, and $\mathbf{x}_p$ is the position of the center of the particle p.

Given three linearly independent strain tensors $\boldsymbol{\varepsilon}^i$ and associated stress tensors $\boldsymbol{\sigma}^i$, the elasticity tensor $\mathbf{E}$ can be expressed as:

$$\mathbf{E}_K = \left(\left[\boldsymbol{\sigma}_K^1, \boldsymbol{\sigma}_K^2, \boldsymbol{\sigma}_K^3 \right] \left[\boldsymbol{\varepsilon}_K^1, \boldsymbol{\varepsilon}_K^2, \boldsymbol{\varepsilon}_K^3 \right]^{-1} \right)^S \tag{12}$$

where $\bullet_K$ denotes the Kelvin notation ($\boldsymbol{\sigma}_K = \left[\sigma_{11}, \sigma_{22}, \sqrt{2}\sigma_{12}\right]^T$). The indicial symmetrization of strain and stress enforces the minor symmetry of elasticity tensor. The symmetrization in Equation 12 enforces the major symmetry of the elasticity tensor.

The loadings are chosen such that Hill's macro-homogeneity condition (also named Hill-Mandel condition) is satisfied (based on Hill's lemma [17], proof available in [18] among others). It states that the average elastic energy in the RAE is equal to the product of average strain and stress. It can be shown that PBC verify Hill's macro-homogeneity condition.

The three linearly independent strain loadings used to measure the elasticity tensor are:

$$\boldsymbol{\varepsilon}_K^1 = \left[\varepsilon, 0, 0\right]^T \qquad \boldsymbol{\varepsilon}_K^2 = \left[0, \varepsilon, 0\right]^T \qquad \boldsymbol{\varepsilon}_K^3 = \left[0, 0, \sqrt{2}\varepsilon\right]^T \tag{13}$$

where ε is sufficiently small to ensure that the loading remains elastic, even when the specimen is cracked.

4.2 Measurement of the evolution of the effective elasticity tensor

The procedure to measure the evolution of the effective elasticity tensor consists in measuring the elasticity tensor at each load step of a damaging loading. Algorithm 1 details this procedure, and Figure 2 illustrates it.

Algorithm 1: Measurement of the evolution of effective elasticity tensor

```
Generate a mesh;
Apply a damaging loading;
for each load step do
    Extract the cracks;
    Add the cracks to the (initial) uncracked mesh;
    for each measurement loading i do
        Apply the strain measurement loading ε^i_K (periodic and elastic);
        Compute the average strain ε^i_K using Equation (10);
        Compute the average stress σ^i_K using Equation (11);
    end
    Compute the effective elasticity tensor using Equation (12);
end
```

[2] Given a 2nd order tensor $\mathbf{t}$, the symmetric part $\mathbf{t}^S$ minimizes $\|\mathbf{t} - \mathbf{t}^*\|$.

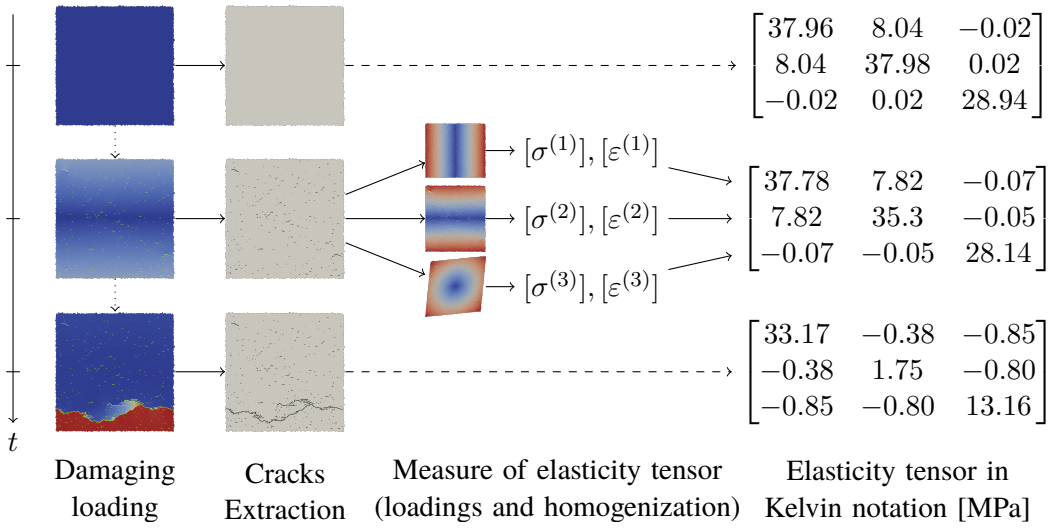

Figure 2: Method to measure the evolution of the effective elasticity tensor

5 Illustration on a tensile loading

A periodic tensile loading is applied onto a square specimen to create an anisotropic cracking pattern. The strain-stress curve as well a cracking patterns are reported in Figure 3.

The strain-stress curve in Figure 3a is composed of different phases. Firstly, an elastic phase during which no micro-cracks appear before point (b). Before point (c), the stiffness starts to decrease slowly: it corresponds to a phase of diffuse micro-cracking. Between point (c) and point (d), mome micro-cracks merge into a macro-crack leading to a significant loss of stiffness. Finally, the macro-crack continue to propagate, leading to further decrease of stiffness.

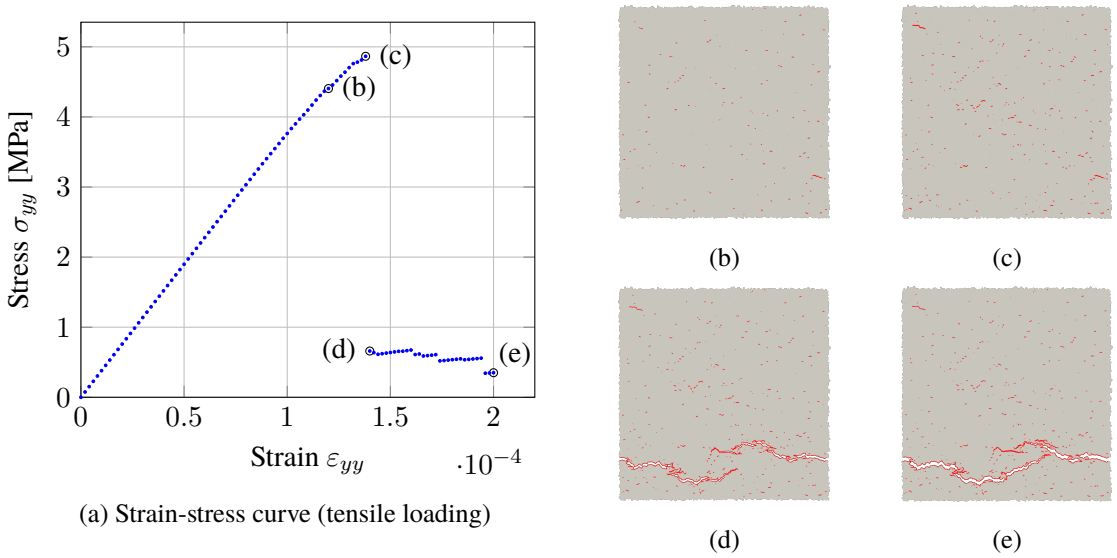

(a) Strain-stress curve (tensile loading)

Figure 3: Illustration of a damaging tensile loading: stress-strain curve and cracking patterns.

The evolution of the elasticity tensor is measured during the loading and shown in Figure 4. The forty first steps corresponds to the elastic phase. During the micro-cracks localization, the isotropic parameters decreases whereas the dilatation part grows significantly. It is a manifestation of the damage-induced anisotropy.

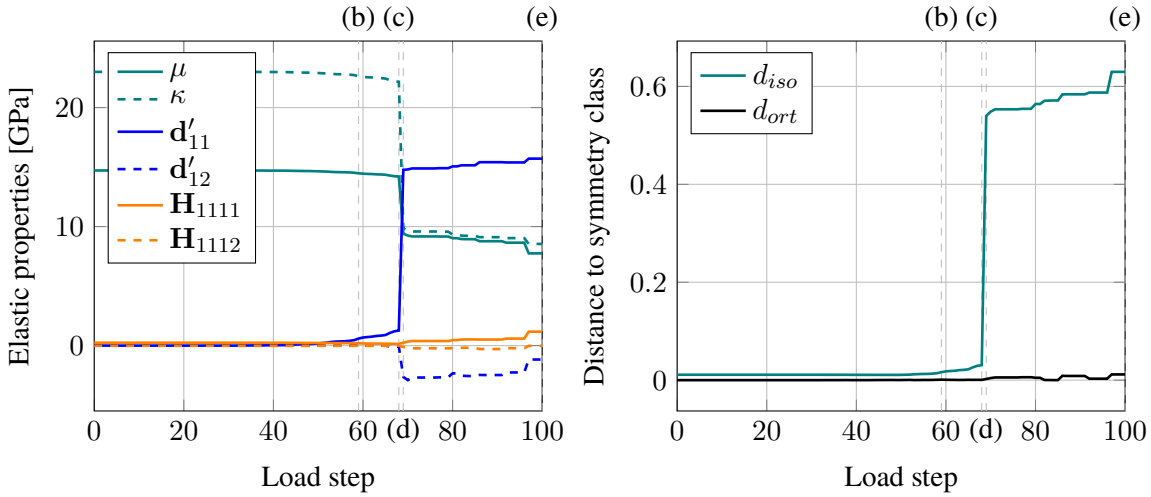

(a) Invariants and covariants

(b) Distance to symmetry classes

Figure 4: Evolution of effective elasticity tensor during tensile loading

This evolution can also be analyzed in terms of distance to symmetry classes, as shown in Figure 4b. It shows that the initial distance to the isotropy class is not zero. The mesh generation procedure can explain it: it is due to the grid used to place the particle centers. Note that a decrease of the average beam length $\bar{l}_b$ leads to a decrease in the distance to isotropy. During the elastic phase and diffuse micro-cracking, the distance to isotropy does not significatively change. However, when micro-cracks merge into a macro-crack, the distance to isotropy abruptly increases. The last observation is that the distance to orthotropy does not grow during the loading. An orthotropic elasticity tensor can reasonably approximate the effective elasticity tensor.

6 Conclusion

A procedure to measure the evolution of the effective elasticity tensor from a beam-particle model have been presented. It provides a flexible framework to study the evolution of damage, based on an explicit representation of micro-cracking. The virtual specimen can be submitted to multi-axial non-proportional loadings while measuring the effective elasticity tensor. It is a complement to experiments as this type of measurements are difficult to carry out. It also enables to scan a large number of damaging loadings with a lesser cost. The harmonic decomposition of the elasticity tensor is used to obtain a parametrization of the elasticity tensor with invariants and covariants. Moreover, calculations of distance to symmetry classes allow to quantify the evolution of anisotropy during a mechanical loading. This framework will be used to formulate a 2D anisotropic damage model based on the harmonic decomposition. The proposed procedure will then be extended to 3D.

References

[1] Mazars J., Berthaud Y., Ramtani S., (1990). The unilateral behaviour of damaged concrete. Engineering Fracture Mechanics 35(4), pp. 629–635.

[2] Ramtani S., Berthaud Y., Mazars J., (1992). Orthotropic behavior of concrete with directional aspects: modelling and experiments. Nuclear Engineering and Design 133(1), pp. 97–111.

[3] Delaplace A., Desmorat R., (2008). Discrete 3D model as complimentary numerical testing for anisotropic damage. International Journal of Fracture 148(2), pp. 115–128.

[4] Rinaldi A., (2013). Bottom-up modeling of damage in heterogeneous quasi-brittle solids. Continuum Mechanics and Thermodynamics 25(2), pp. 359–373.

[5] Wriggers P., Moftah S.O., (2006). Mesoscale models for concrete: Homogenisation and damage behaviour. Finite Elements in Analysis and Design 42(7), pp. 623–636.

[6] D'Addetta G. A., Kun F., Ramm E., (2002). On the application of a discrete model to the fracture process of cohesive granular materials. Granular Matter 4(2), pp. 77–90.

[7] Vassaux M., Oliver-Leblond C., Richard B., Ragueneau F., (2016). Beam-particle approach to model cracking and energy dissipation in concrete: Identification strategy and validation. Cement and Concrete Composites 70, pp. 1–14.

[8] Hrennikoff A., (1941). Solution of problems of elasticity by the framework method. Journal of Applied Mechanics 8(4), pp. A169–175.

[9] Herrmann H. J., Hansen A., Roux S., (1989). Fracture of disordered, elastic lattices in two dimensions. Physical Review B 39(1), pp. 637–648.

[10] Schlangen E., van Mier J. G. M., (1992). Simple lattice model for numerical simulation of fracture of concrete materials and structures. Materials and Structures 25(9), pp. 534–542.

[11] Cundall P. A., Strack O. D. L., (1979). A discrete numerical model for granular assemblies. Géotechnique 29(1), pp. 47–65.

[12] Oliver-Leblond C., Desmorat R., Kolev B., (2021). Continuous anisotropic damage as a twin modelling of discrete bi-dimensional fracture. European Journal of Mechanics - A/Solids 89, 104285.

[13] Backus G., (1970). A geometrical picture of anisotropic elastic tensors. Reviews of Geophysics 8(3), pp. 633–671.

[14] Antonelli A., Desmorat B., Kolev B., Desmorat R., (2022). Distance to Plane Elasticity Orthotropy by Euler-Lagrange Method. arXiv. Working paper or preprint.

[15] Bagi K., (2006). Analysis of microstructural strain tensors for granular assemblies. International Journal of Solids and Structures 43(10), pp. 3166–3184.

[16] Bagi K., (1996). Stress and strain in granular assemblies. Mechanics of Materials 22(3), pp. 165–177.

[17] Hill R., (1963). Elastic properties of reinforced solids: Some theoretical principles. Journal of the Mechanics and Physics of Solids 11(5), pp. 357–372.

[18] Qu J., Cherkaoui M., (2006). Fundamentals of Micromechanics of Solids. John Wiley & Sons, Inc.